PLEASE CITE THIS ARTICLE AS DOI: 10.1063/5.0226758

## Shear-driven stability of a rigid particle in yield stress fluids

Rakan Alrashdan<sup>1</sup> and Fardin Khabaz\*<sup>1,2</sup>

<sup>1)</sup>School of Polymer Science and Polymer Engineering, The University of Akron, Akron, OH, 44325, United States.

<sup>2)</sup>Department of Chemical, Biomolecular, and Corrosion Engineering,

The University of Akron, Akron, OH, 44325, United States.

(\*Electronic mail: fkhabaz@uakron.edu)

(Dated: 13 September 2024)

The stability of a rigid particle in yield stress fluids, comprised of soft particle glasses (SPGs), is investigated in shear flow under an applied external force, such as weight, using particle dynamics simulations. Results provide the critical force threshold, in terms of the dynamic yield stress and the flow strength, required to initiate sedimentation of the rigid particle over a wide range of shear rates and volume fractions. The streamlines of the SPGs show local disturbances when the rigid particle settles. The form of these disturbances is consistent with the microdynamics and microstructure response of the neighboring soft particles of the sedimenting rigid particle. Sedimenting particle induces non-affine displacement to the suspensions at low shear rates and high applied forces, while these dynamical events are localized and suppressed at high shear rates. Stability diagrams, which provide the conditions of the sedimentation of the rigid particle are presented in terms of the applied force and the shear rate. These individual stability diagrams at each volume fraction map onto a universal stability diagram when the external force is scaled by the dynamic yield stress and shear rate with a ratio of the solvent viscosity to the low frequency modulus of the SPGs.

This is the author's peer reviewed, accepted manuscript. However, the online version of record will be different from this version once it has been copyedited and typeset PLEASE CITE THIS ARTICLE AS DOI: 10.1063/5.0226758

Stability of rigid particle in yield stress fluids

## I. Introduction

Yield stress fluids, such as soft particle glasses (SPGs),  $^{1-7}$  which can be in the form of concentrated emulsions, microgels, and star polymers with many arms, are deformable particles and are jammed beyond the random close packing of equivalent hard sphere suspensions,  $^8$  *i.e.*,  $\phi_{rcp} = 0.64$ . Distinct from hard sphere glasses, which experience forces only to excluded volume interactions, SPGs compress due to a bulk osmotic force and interact *via* an elastic repulsive potential.  $^{1,6,7}$  These suspensions behave like weak elastic solids at rest but flow macroscopically and exhibit shear thinning behavior under the application of stresses larger than a stress value known as the dynamic yield stress  $\sigma_y$ .  $^{3,4,6,9-11}$  The shear rate dependence of the shear stress is often expressed by the Herschel-Bulkley (HB) equation,  $\sigma = \sigma_y + k\gamma^n$ , where n is the exponent close to 0.5, and k is the consistency parameter.  $^{3,10,12,13}$  SPGs show industrial importance as rheological additives and arise in industrial processes such as concrete casting, drilling muds,  $^{14,15}$  and share similarities with natural phenomena like debris-flow and lava-flow. These processes usually contain rigid particles that tend to settle under the influence of gravity or other disturbances like shear forces,  $^{16}$  resulting in altered material properties and phase separation.  $^{17,18}$ 

The flow curve of these SPGs exhibits two regimes in which different flow behaviors are expected. 12,13 The first regime, known as quasi-static regime, exhibits a low-shear plateau followed by an upturn and power law region at high shear rates, known as the flow regime. In the quasi-static regime, the occurrence of avalanches, where particles experience sudden movements or rearrangements, suggests a complex interplay of contact and shear forces at the microscopic level. 13 Conversely, as the shear rate increases, a distinct change in dynamics is observed. The flow becomes more localized, indicating a shift from the cooperative, avalanche-driven behavior of the quasi-static regime to a more localized flow pattern. This transition highlights the fluid's adaptability to varying external conditions and emphasizes the importance of understanding the dual nature of its rheological response. The two different regimes can have different effects on the sedimentation. Understanding the microscopic dynamics in this regime is essential for predicting how particles interact during sedimentation.

Besides the intriguing rheological characteristics of SPGs, the stability of rigid particles, commonly used as functional additives in SPGs is of interest in various applications. <sup>19–21</sup> This aspect brings up essential inquiries into the interactions between soft and rigid particles when activated by shear, particularly above the jamming transition. This phenomenon involves rigid particles in

## This is the author's peer reviewed, accepted manuscript. However, the online version of record will be different from this version once it has been copyedited and typeset. PLEASE CITE THIS ARTICLE AS DOI: 10.1063/5.0226758

Stability of rigid particle in yield stress fluids

yield stress fluids settling through the suspended fluid undergoing shear flow. This process has the potential to induce phase separation and alter material properties. If the sedimentation rate can be predicted or modified, it becomes possible to design fluids with tailored properties, such as enhanced stability. Moreover, the microstructure of these particles shows significant importance in governing the sedimentation dynamics. Sedimentation rates of monodisperse disordered suspensions consisting of rigid particles at volume fraction  $\phi \leq 0.50$  shows that the spatial configuration and the hydrodynamic interactions of the particles within the fluid plays a critical role in determining the sedimentation rate. Furthermore, previous work<sup>23</sup> highlights the effect of the fluid's microstructure on sedimentation by examining a colloidal glass like *Carbopol* where the particles are polydisperse with a submicron size domain, and a colloidal gel like microfibrillous cellulose and found that despite having the same yield stress, they exhibit a six-fold difference in their ability to offset a given particle stress. Therefore, microfibrillous cellulose exhibits a more suspension ability than *Carbopol* as a result of microstucture differences. Under quiescent conditions, at volume fraction above jamming transition, the forced motion of a soft particle has been previously studied and it has been found that the external force effects the sedimentation behavior.  $^{25}$ 

In shear-induced sedimentation  $^{16,26}$  in suspensions with volume fraction  $\phi=0.05$ , the sedimentation velocity is not only a function of their inherent properties but also of the applied shear conditions, suggesting avenues for manipulating sedimentation through external forces. Furthermore, the interplay between the yielding behavior of the fluid and the imposed shear conditions can lead to varied sedimentation dynamics. The elasticity of the fluid modifies the drag on the settling particle, potentially reducing it in comparison to a purely viscoplastic medium. This understanding allows for tailored fluid properties to achieve desired sedimentation outcomes by adjusting the balance between elastic and plastic effects within the fluid. In this regard, a comprehensive analysis of shear-induced migration in yield stress fluids, emphasizing how the interplay between particle dynamics and fluid rheology under shear conditions can be manipulated to control sedimentation processes was provided. This migration is influenced by the shear gradient across the fluid, forcing particles to relocate from areas of high to low shear stress. This movement significantly alters sedimentation patterns and overall suspension stability. Furthermore, variations in shear rates across the fluid lead to non-uniform particle distributions, which are pivotal in determining the stability and uniformity of suspensions.

The dynamics of particle sedimentation in yield stress fluids undergo distinct transformations in confinement due to the restricted spatial conditions, which directly influence the flow and stress

PLEASE CITE THIS ARTICLE AS DOI: 10.1063/5.0226758

distribution around the particles. Confinement intensifies the asymmetry in flow fields and alters the typical yield surfaces, forming ovoid spheroid shapes that are more pronounced compared to unconfined environments.<sup>29</sup> These observations suggest that the flow patterns and mechanical stresses on the particle are significantly influenced by the proximity of boundaries, which can modify the fluid's yielding behavior and the sedimentation process. The sedimentation of spherical PMMA particles suspended in a mixture of *Carbopol*<sup>®</sup>, water, and glucose, flowing in a horizontal cylindrical pipe under two scenarios were considered.<sup>30</sup> The first scenario, which neutralized the effects of gravity, demonstrated that the particles did not undergo radial migration during flow. In contrast, the second scenario, involving particles denser than the fluid, revealed that gravity's influence became significant. Notably, while particles in the plug flow zone remained suspended, those in the sheared zone settled. The understanding of sedimentation dynamics in flows is crucial for designing and optimizing processes in various engineering applications, including the formulation of drilling muds in narrow boreholes and the management of waste in constrained pathways, where control over sedimentation and flow characteristics is essential.

The problem of sedimentation and stability of suspensions becomes challenging in yield stress fluids comprised of SPGs since their dynamics is strongly shear dependent. 13 The occurrence of avalanches might lead to non-uniform settling, impacting the overall sedimentation process at the quasi-static regime of flow. As the yield stress fluid transitions to the flow regime at higher shear rates, the sedimentation dynamics can change. During sedimentation, this transition signifies a shift from a state where particles experience intermittent avalanches to a more continuous, directed settling. Advanced understanding of sedimentation dynamics allows for the optimization of formulations, ensuring that products meet the desired standards over time. In industrial contexts, sedimentation of particles in yield stress fluids like Carbopol®, holds particular significance due to its direct impact on shelf life of products. 31-35 The undesired settling of particles can result in uneven distribution of components, adversely affecting the overall quality and stability of the products over time. Advanced understanding and control of sedimentation dynamics enable the development of strategies to mitigate its effects, ensuring that the particles remain uniformly distributed throughout the fluid. This, in turn, contributes to the overall stability and prolonged shelf life, given the fact that nearly 40% of the cost of developing a new emulsion product is incurred in testing the shelf life.<sup>36</sup> Previous work<sup>31</sup> investigated sedimentation of suspensions and Pickering emulsions in relation to their shelf life and emphasized the significant role of nanoparticlestabilized interfaces in altering the behaviors of these systems, with the three-phase contact angle

PLEASE CITE THIS ARTICLE AS DOI: 10.1063/5.0226758

## being a critical factor.

The dynamics of sedimentation are a function of mechanical disturbances from soft particle contacts at both low and high shear rates. Consequently, the volume fraction of the SPGs, along with the interactions between soft and rigid particles and the strength of the flow, are crucial factors in determining the stability of these suspensions. In this regard, we study the microstructure and dynamics of sedimentation formed by polydisperse jammed particles and a single rigid particle. Specifically, our objectives are: (1) to understand the affect of applying a force on the dynamics of sedimentation of the rigid particle in shear flow, (2) to determine the velocity field of the SPGs at the vicinity of the rigid particle, and (3) to provide universal stability diagrams and stability criterion where the effect of varying applied force, volume fraction, and shear rate is considered. To pursue these objectives, we employ three-dimensional (3D) particle simulations, <sup>1,10</sup> and explore the impact of varying applied force and shear rate on rigid particle sedimentation in steady shear flow. Our results show that aside from volume fraction, the sedimentation is governed by dynamic yield stress, particle radius, and shear rate.

## II. Simulation details and method

## A. Suspensions specifications

10,000 particles, one of which is a rigid particle and the rest are soft, with a polydispersity index of  $\delta = 0.2$ , are suspended in a Newtonian liquid with a viscosity  $\eta_s$  at volume fractions in the range of  $0.70 \le \phi \le 0.90$  (Fig. 1(A)).

## B. Force law and shear flow protocol

Following previous works,  $^{1,10}$  we utilize the methodology for simulating SPGs in shear flow using our in-house parallel code, where the normal contact elastic force,  $\mathbf{F}^{E}_{\alpha\beta}$ , between soft particles is governed by the Generalized Hertz law<sup>3,4,10</sup> according to:

$$\mathbf{F}_{\alpha\beta}^{E} = \frac{4}{3} E^* \varepsilon_{\alpha\beta}^{n} R_c^2 \mathbf{n}_{\perp},\tag{1}$$

where  $E^*$  is the contact modulus of two particles at contact and is equal to  $1/E^* = (1 - v_\alpha^2)/E_\alpha + (1 - v_\beta^2)/E_\beta$ , where v and E are the Poisson ratio and elastic modulus of a given particle. When a soft and rigid particle (i.e., particle  $\beta$ ) comes in contact, we consider  $E_\beta \longrightarrow \infty$ , and the contact modulus of the rigid-soft interaction will then become  $E^* = E/(1 - v^2)$ . In this expression,  $\varepsilon_{\alpha\beta}$  is the dimensionless overlap parameter which is defined as  $\varepsilon_{\alpha\beta} = (R_\alpha + R_\beta - r_{\alpha\beta})/R_c$ , where  $R_c = R_\alpha R_\beta/(R_\alpha + R_\beta)$  is the effective radius of the two particles in contact and  $r_{\alpha\beta}$  is the distance between particles  $\alpha$  and  $\beta$ .  $\mathbf{n}_\perp$  is the normal vector to the facets at contact as shown in Fig. 1(B).

PLEASE CITE THIS ARTICLE AS DOI: 10.1063/5.0226758

Stability of rigid particle in yield stress fluids

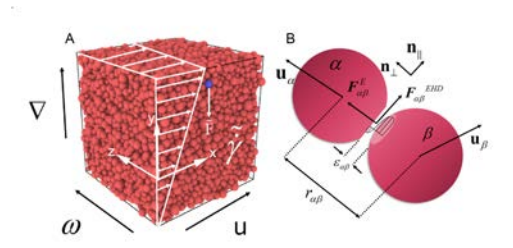


FIG. 1. (A) Configuration of a polydisperse suspension with a volume fraction of  $\phi=0.80$  subjected to shear flow with an applied shear rate of  $\tilde{\gamma}$  in a periodic simulation box. The applied force,  $\tilde{F}=\frac{F}{R^2E^*}$  exerted on the rigid particle (blue color) in the negative gradient direction ( $\nabla$ ). The velocity ( $\mathbf{u}$ ), gradient ( $\nabla$ ), and vorticity ( $\omega$ ) directions are indicated. The sedimentation results are independent of the vertical placement of the rigid particle in the simulation box since periodic boundary conditions are applied. (B) Schematic representation of the pair-wise contact between particles  $\alpha$  and  $\beta$ .

Thus, our current methodology can predict the dynamics of a single rigid particle in the SPGs phase under shear flow.

Two particles in contact also experience elastohydrodynamic force,  $\mathbf{F}_{\alpha\beta}^{EHD}$ , 37 according to:

$$\mathbf{F}_{\alpha\beta}^{EHD} = -(\eta_s u_{\alpha\beta\parallel} E^* R_c^3) \varepsilon_{\alpha\beta}^{(2n+1)/4} \mathbf{n}_{\parallel}, \tag{2}$$

where  $u_{\alpha\beta\parallel}$  is the magnitude of the relative velocity of two particles in the direction parallel to the facets in contact, *i.e.*,  $\mathbf{n}_{\parallel}$ . The vector  $\mathbf{n}_{\parallel}$  lies in the tangential plane at the contact point. Its specific direction within this plane is critical for modeling the sliding interactions that occur when particles move relative to each other under shear, and usually, this alignment is parallel to the shear direction, ensuring that the EHD force represents the shear-driven relative velocities of the particles along the contact plane. This particular orientation is necessary for calculating the component of relative velocity that is tangential to the point of contact,  $\mathbf{u}_{\mathbf{n}_{\parallel}}^{rel}$ , which is given by  $\mathbf{u}_{\mathbf{n}_{\parallel}}^{rel} = \mathbf{u}_{\parallel} - (R_{\alpha}\Omega_{\alpha} + R_{\beta}\Omega_{\beta}) \times \mathbf{n}_{\perp}$ , where  $\mathbf{u}_{\parallel} = \mathbf{u}_r - \mathbf{u}_r \cdot \mathbf{n}_{\perp}\mathbf{n}_{\perp}$ ,  $\mathbf{u}_r$  is the relative velocity ( $\mathbf{u}_r = \mathbf{u}_{\beta} - \mathbf{u}_{\alpha}$ ), and  $\Omega_{\alpha}$  and  $\Omega_{\beta}$  are the angular velocities of the particles  $\alpha$  and  $\beta$ . In our suspensions, since the volume fraction is high, the rotational motion of our particles is limited, therefore,  $\mathbf{u}_{\mathbf{n}_{\parallel}}^{rel} = \mathbf{u}_{\parallel}$ . Thus, the direction of the applied force is  $\mathbf{n}_{\parallel} = \frac{\mathbf{u}_{\mathbf{n}_{\parallel}^{rel}}}{||\mathbf{u}_{\mathbf{n}_{\parallel}^{rel}}^{rel}||}$ . Furthermore, the rigid particle experiences a applied force  $\mathbf{F}^{AF}$  according to:

$$\mathbf{F}^{AF} = -F\mathbf{e}_{\mathbf{y}} \tag{3}$$

PLEASE CITE THIS ARTICLE AS DOI: 10.1063/5.0226758

This is the author's peer reviewed, accepted manuscript. However, the online version of record will be different from this version once it has been copyedited and typeset

where  $\mathbf{e}_{v}$  is the basis vector in the gradient direction.

Considering these three forces and using the scales of the particle size R and time  $\eta_s/E^*$ , the dimensionless equation of motion for the particle  $\alpha$  in shear flow becomes:

$$\frac{d\tilde{\mathbf{x}}_{\alpha}}{d\tilde{t}} = \mathbf{u}_{\alpha}^{\infty} + \frac{\mathbf{M}}{\tilde{R}_{\alpha}} \cdot \left( \tilde{\mathbf{F}}_{\alpha\beta}^{E} + \tilde{\mathbf{F}}_{\alpha\beta}^{EHD} + \tilde{\mathbf{F}}^{AF} \right), \tag{4}$$

where  $\mathbf{M} = \frac{f(\phi)}{6\pi}\mathbf{I}$  is the mobility coefficient, which is that of a particle corrected by  $f(\phi)$  that accounts for its reduction at high volume fraction, and is set to  $0.01.^{7,10}$   $\mathbf{u}_{\alpha}^{\infty}$  describes the shear advection velocity of a particle  $\alpha$ . Forces are scaled by  $R^2E^*$ , *i.e.*,  $\tilde{\mathbf{F}} = \frac{\mathbf{F}}{R^2E^*}$ , and  $\tilde{\mathbf{F}}^{AF}$  has a value of 0 when both contacts are soft. Note that the dimensionless shear rate of  $\tilde{\gamma} = \frac{\dot{\gamma}\eta_s}{E^*}$  in the range of  $10^{-8} - 10^{-3}$  is used to impose the shear rate on the suspensions by applying the Lees–Edwards boundary conditions.<sup>38</sup> The dimensionless applied force of  $0.01 \le \tilde{F} \le 1.00$  is applied to the rigid particle in the direction of the gradient of flow. The stress tensor is then computed as a function of time using the Kirkwood formula, *i.e.*,  $\sigma = \frac{1}{L^3} \Sigma_{\alpha} \Sigma_{\beta} \mathbf{F}_{\alpha\beta} (\mathbf{x}_{\alpha} - \mathbf{x}_{\beta})$ , where  $\mathbf{F}_{\alpha\beta}$  is the total force exerted on particle  $\alpha$  by particle  $\beta$ , and L is the length of the cubic box.<sup>39</sup> In all simulations, the suspensions are subjected to shear flow for 10 strains.

## III. Results and discussion

## A. Dynamics and microstructure

We track the trajectories of the rigid particle in three-dimensional space at different shear rates and applied forces on the rigid particle to observe its sedimentation. In Fig. 2A, the trajectories of the rigid particle at a high shear rate of  $\tilde{\gamma}=10^{-3}$  and an applied force of  $\tilde{F}=0.01$  are shown for a strain duration of  $\gamma=10$ . At this high shear rate, the trajectory of this particle is notably more localized and the sedimentation in the direction of the external force is suppressed; suggesting a strong influence of shear rate on the dynamics of sedimentation. At  $\tilde{\gamma}=10^{-7}$  at the same  $\tilde{F}$  value, the rigid particle exhibits a dispersed trajectory as shown in Fig. 2B. This trajectory shows the sedimenting rigid particle travels a significant distance in the direction of the applied force, highlighting the impact of shear rate on particle motion.

This is the author's peer reviewed, accepted manuscript. However, the online version of record will be different from this version once it has been copyedited and typeset PLEASE CITE THIS ARTICLE AS DOI: 10.1063/5.0226758

## Stability of rigid particle in yield stress fluids

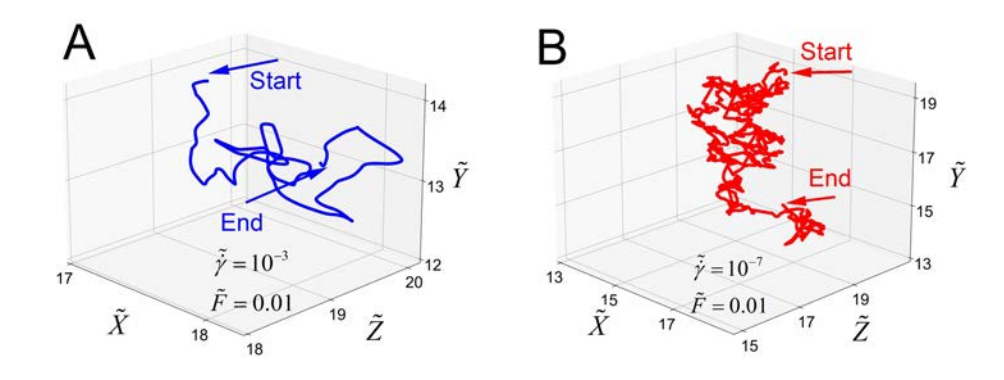


FIG. 2. Trajectories of the rigid particle in shear flow with an applied force of  $\tilde{F}=0.01$  and at (A)  $\tilde{\gamma}=10^{-3}$  and (B)  $\tilde{\gamma}=10^{-7}$  for a strain duration of  $\gamma=10$ .

Building on these observations, the correlation between the sedimentation velocity,  $\tilde{V}_{\nu}$ , and shear rate,  $\tilde{\gamma}$ , at different applied force,  $\tilde{F}$ , and volume fractions is presented in Fig. 3.  $\tilde{V}_{\nu}$  of the sedimenting rigid particle increases across a range of volume fractions and applied force. The general trend observed throughout the panels is that the velocity increases with the increase in shear rate and applied force. While this increase is partially due to the applied force, it is also significantly influenced by the shear-induced diffusive motion that intensifies with higher shear rates.<sup>3</sup> This enhanced diffusive behavior contributes to the overall dynamics of the system, where the shear-induced diffusion coefficient is shown to increase with shear rate. When the velocity is rescaled with shear rate,  $V_v/\dot{\gamma}R$ , the rescaled sedimentation velocity decreases with the increase in shear rate at all volume fractions. Slower sedimentation velocity at lower shear rates reflects an enhanced resistance against particle settling. This is similar to the trend reported in the experimental work by Overlez et al. 16,40 where the sedimentation velocity of glass beads of varying diameters undergoing shear flow increased with both shear rate and particle diameter. Furthermore, at a constant force, a decrease in  $\tilde{V_y}$  with the increase in volume fraction, where the hindrance from particle packing is more significant, is observed in Figs. 3A, 3B and 3C. The yield stress increases with volume fraction; therefore, at a given shear rate and applied force, the effective strength of the increased volume fraction prevents the sedimentation of the rigid particle. This finding aligns with the results obtained by Brady and Durlofsky<sup>22</sup> in monodisperse hard sphere suspension in a quiescent condition at different volume fractions, where the increased

PLEASE CITE THIS ARTICLE AS DOI: 10.1063/5.0226758

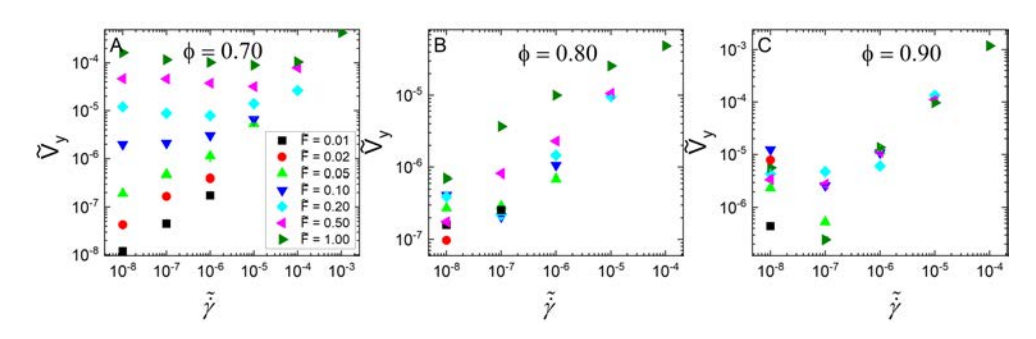


FIG. 3. Sedimentation velocity of the sedimenting particle,  $\tilde{V}_y$ , where  $\tilde{V}_y$  is defined as  $\tilde{V}_y = \frac{V_y \eta_s}{E^* R}$ , at different shear rates with volume fraction of (A)  $\phi = 0.70$ , (B)  $\phi = 0.80$ , and (C)  $\phi = 0.90$ .

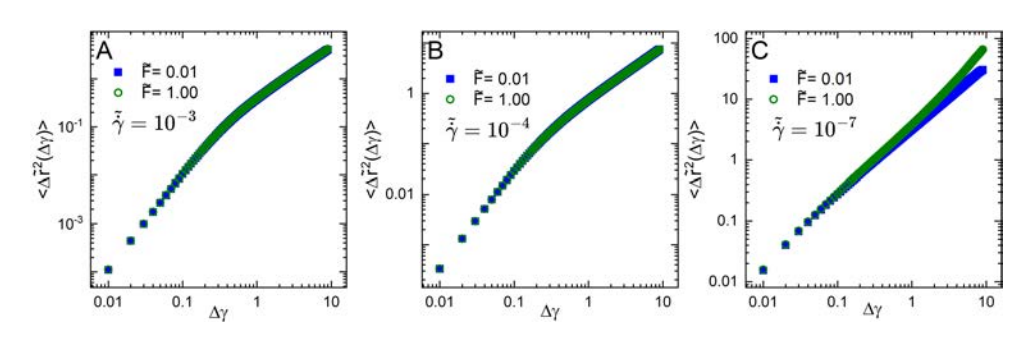


FIG. 4. Mean squared displacement, (MSD),  $<\Delta \tilde{r}^2(\Delta \gamma)>$ , of a suspension with volume fraction  $\phi=0.80$  at (A)  $\tilde{\gamma}=10^{-3}$ , (B)  $\tilde{\gamma}=10^{-4}$ , and (C)  $\tilde{\gamma}=10^{-7}$ . The applied force values are  $\tilde{F}=0.01$  and  $\tilde{F}=1.00$ .

volume fraction of suspensions favors a slower sedimentation velocity.

To measure the distance that particles have moved over time under varying shear conditions and applied forces, the mean squared displacement (MSD),  $<\Delta\tilde{r}^2(\Delta\gamma)>$ , are presented in Fig. 4. and provides a quantitative measure of how particles displacement is influenced by external forces across different forces and shear rates, offering insights in the dynamics that drive the macroscopic behaviors observed in Fig. 3. In Fig. 4(A), under a high shear rate of  $\tilde{\gamma}=10^{-3}$  and two different applied forces of  $\tilde{F}=0.01$  and  $\tilde{F}=1.00$ , the MSD shows no force dependence. Similarly in Fig. 4(B), there is a greater displacement, however, MSD seems to be force independent at high shear rates. Furthermore, Fig. 4(C) shows a distinct break-off when a force of  $\tilde{F}=1.00$  is applied. At this low shear rate, the MSD at this applied force increases with the increase in applied force,

This is the author's peer reviewed, accepted manuscript. However, the online version of record will be different from this version once it has been copyedited and typeset PLEASE CITE THIS ARTICLE AS DOI: 10.1063/5.0226758

## Stability of rigid particle in yield stress fluids

which suggests that at low shear rates, external forces can induce significant particle movements, potentially leading to fast sedimentation dynamics and enhancing dynamics of nearby particles. Hence, the largest  $\tilde{V}_{\nu}$  is observed at  $\tilde{F}=1.00$ .

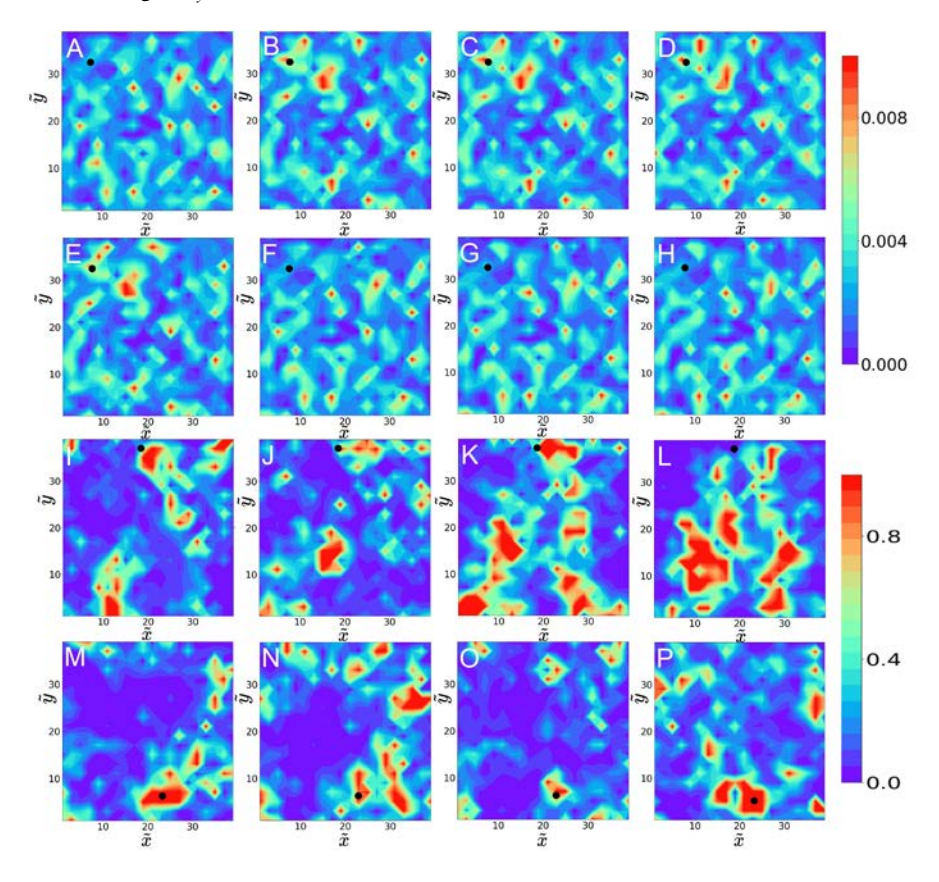


FIG. 5. Non-affine squared displacement parameter,  $D_m^2$ , at consecutive strains in the steady state for suspensions with volume fraction  $\phi=0.80$  undergoing  $\tilde{\gamma}=10^{-3}$  and  $\tilde{F}=0.01$  (A-D),  $\tilde{\gamma}=10^{-3}$  and  $\tilde{F}=1.00$  (E-H),  $\tilde{\gamma}=10^{-7}$  and  $\tilde{F}=0.01$  (I-L) and  $\tilde{\gamma}=10^{-7}$  and  $\tilde{F}=1.00$  (M-P).  $D_m^2$  values of each particle were calculated over a strain interval of  $\Delta\gamma=0.01$ . The color bar provides the spectrum of the  $D_m^2$  values with red and blue limits corresponding to the maximum and zero  $D_m^2$ , respectively. The rigid particle is shown with a black circle.

A crucial question that still needs to be addressed is whether the rigid particle moves indepen-

PLEASE CITE THIS ARTICLE AS DOI: 10.1063/5.0226758

This is the author's peer reviewed, accepted manuscript. However, the online version of record will be different from this version once it has been copyedited and typeset

dently or if its motion is correlated with the movements of the soft ones. To address this question, we compute the local strain field in the neighborhood of any particle. The local strain field<sup>41</sup> is determined by minimizing the mean squared difference between the displacements of the neighboring particles relative to the central one and the relative displacements that they would have if they were in a region of uniform strain  $\varepsilon_{ij}$ . The non-affine squared displacement parameters,  $D_m^2$ , which describes the local deviation from affine deformation during a specified strain interval is obtained by

$$D^{2}(\gamma,\Delta\gamma) = \sum_{n} \sum_{i} (r_{n}^{i}(\gamma) - r_{0}^{i}(\gamma) - \sum_{j} (\delta_{ij} + \varepsilon_{ij}) (r_{n}^{j}(\gamma - \Delta\gamma) - r_{0}^{j}(\gamma - \Delta\gamma)))^{2}.$$
 (5)

In Eq.(5), i and j are spatial coordinates and the index n runs over the particles within the the first neighbors of the reference particle.  $r_n^i(\gamma)$  is the i-th component of the position vector of the n-th particle at strain of  $\gamma$ . By minimizing this function, the local strain field is determined:

$$\varepsilon_{ij} = \sum_{k} (X_{ij} Y_{ij}^{-1} - \delta_{ij}), \tag{6}$$

where index k is used to denote the summation over the components contributing to the local strain field from the surrounding particles such as spatial coordinates or directions that are involved in the calculation of the strain tensor and  $X_{ij}$  and  $Y_{ij}$  are given as

$$X_{ij} = \sum_{n} (r_n^i (\gamma - \Delta \gamma) - r_0^i (\gamma - \Delta \gamma)) (r_n^j (\gamma - \Delta \gamma) - r_0^j (\gamma - \Delta \gamma)) \text{ and}$$

$$Y_{ij} = \sum_{n} (r_n^i (\gamma) - r_0^i (\gamma)) (r_n^j (\gamma - \Delta \gamma) - r_0^j (\gamma - \Delta \gamma)).$$
(7)

The minimum value of  $D^2(\gamma,\Delta\gamma)$  corresponds to  $D_m^2$  which quantifies the local deviation from affine deformation during the strain interval of  $(\gamma-\Delta\gamma,\gamma)$ . Fig. 5 shows color maps of  $D_m^2$  values with varying shear rate and applied force. At a high shear rate of  $\tilde{\gamma}=10^{-3}$  and an applied force values of  $\tilde{F}=0.01$  and  $\tilde{F}=1.00$ , there is a weak dynamical correlation between the rigid and soft particles and the flow is localized as seen in Figs. 5(A-H). The rigid particle causes local disturbances to the neighboring soft particles at high shear rates, and the dynamics of the yield stress fluid suppresses propagation. However, when decreasing the shear rate to  $\tilde{\gamma}=10^{-7}$  at an applied force of  $\tilde{F}=0.01$ , it is apparent that the rigid particle causes larger disturbances, and there is an increase in mobility that is propagating and transfering to nearby particles as seen in Figs. 5(I-L). Finally, at an applied force of  $\tilde{F}=1.00$ , the heterogeneities in the dynamics caused by the rigid particles are more apparent, confirming that at low shear rate, the motion of the rigid particle is coordinated with the soft ones as observed in Figs. 5(M-P).

PLEASE CITE THIS ARTICLE AS DOI: 10.1063/5.0226758

Stability of rigid particle in yield stress fluids

In order to obtain a deeper insight into the behavior SPGs near the rigid particle in the flowgradient plane, the streamlines of the vicinity of the rigid particle are plotted in Fig. 6 under varying shear rates and applied forces. Fig. 6(A) and Fig. 6(D) show streamlines near a nonsedimenting particle at a shear rate of  $\tilde{\gamma} = 10^{-3}$  with an applied force of  $\tilde{F} = 0.01$  and  $\tilde{F} = 0.01$ 1.00, respectively. The streamlines of these selected suspensions show a shear flow pattern with noticeable circulation zones that inhibit particle settling. In contrast, Fig. 6(B) and Fig. 6(E) show streamlines for a stable and a sedimenting particle, respectively, where the shear rate is decreased to  $\tilde{\gamma} = 10^{-4}$  at the same applied forces investigated at high shear rates. For the stable suspension, the streamlines are similar to those observed in Fig. 6(A) representing typical shear flow, while Fig. 6(E) shows that the rigid particle is sedimenting in the direction of the applied force. Finally, these suspensions show a more disrupted flow pattern as observed in Fig. 6(C) and Fig. 6(F) at shear rate of  $\tilde{\gamma} = 10^{-7}$ . However, in Fig. 6(F) the streamlines show that the SPGs are moving upwards, creating a channel-like effect for the rigid particle to sediment through. This is an indication that the velocity of the rigid particle in the direction of the applied force is significantly greater than the velocity in the flow direction, i.e.,  $\tilde{V}_{\nu} \gg \tilde{V}_{x}$ . This behavior highlights how the varying the applied force and shear rate influences the sedimentation dynamics. The intensified applied force of  $\tilde{F}=1.00$  pushes the particles more towards the applied force path, causing an increase in the local volume fraction, as also noted by Brady and Durlofsky<sup>22</sup> where increased forces led to denser packing and slowed sedimentation due to enhanced particle-particle interactions.

The complex interplay between shear rates, applied force and particle sedimentation is further explored through the analysis of the two-dimensional (2-D) pair distribution  $g(\tilde{x}, \tilde{y})$ , determined in the flow-gradient plane, and the polar distribution function  $g(\tilde{r},\theta)$  between the rigid particle and the SPGs in Figs. 7, 8 and 9. Since there is only a single rigid particle in the suspension and to enhance averaging, 12000 configurations were used which correspond to a strain of  $\gamma = 1000$ in order to capture the microstructure with reasonable accuracy.  $g(\tilde{x}, \tilde{y})$  provides insights into the microstructural organization of particles within suspensions under flow while  $g(\tilde{r}, \theta)$  quantifies the angular asymmetry caused by accumulation and depletion of particles around a reference particle which is the rigid one here. Typically, at high shear rates,  $g(\tilde{x}, \tilde{y})$  tends to show uniform contacts distribution at rest in equilibrium. As the strain increases, an accumulation of particles along the compressive quadrant is observed.<sup>4</sup> On other hand, at lower shear rates, the distribution is more isotropic, reflecting less accumulation and more uniform particle interactions in all directions. This regular behavior serves as a baseline for understanding the modifications induced by the

This is the author's peer reviewed, accepted manuscript. However, the online version of record will be different from this version once it has been copyedited and typeset PLEASE CITE THIS ARTICLE AS DOI: 10.1063/5.0226758

Stability of rigid particle in yield stress fluids

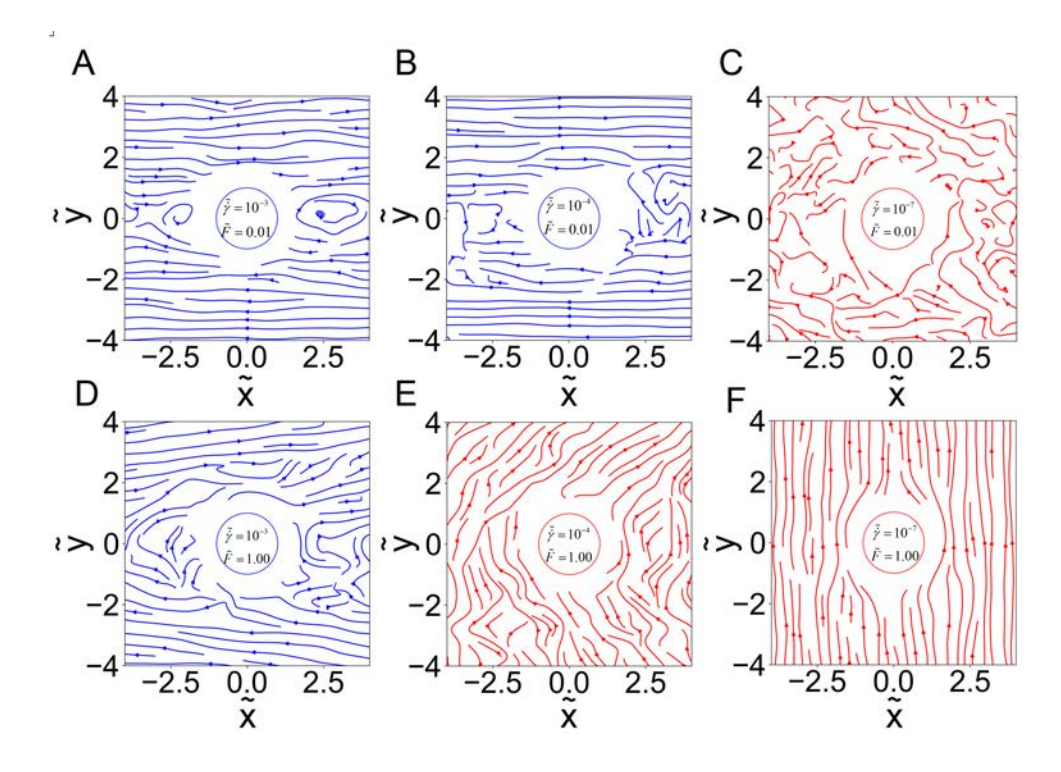


FIG. 6. Velocity streamlines in the vicinity of the rigid particle for a suspension with volume fraction  $\phi=0.80$  undergoing (A)  $\tilde{\gamma}=10^{-3}$  and  $\tilde{F}=0.01$ , (B)  $\tilde{\gamma}=10^{-4}$  and  $\tilde{F}=0.01$ , (C)  $\tilde{\gamma}=10^{-7}$  and  $\tilde{F}=0.01$ , (D)  $\tilde{\gamma}=10^{-3}$  and  $\tilde{F}=1.00$  (E)  $\tilde{\gamma}=10^{-4}$  and  $\tilde{F}=1.00$  and (F)  $\tilde{\gamma}=10^{-7}$  and  $\tilde{F}=1.00$ .

presence of rigid particles in a suspension of softer particles.  $g(\tilde{x}, \tilde{y})$  indicates a region where particles are interacting more intensely, *i.e.*, the rigid particle is experiencing more contacts with the soft particles due to flow-induced dynamics. Fig. 7(A) shows less contacts between rigid and soft particles when  $\tilde{F} = 0.01$  compared to that of  $\tilde{F} = 1.00$  (Fig. 7(C)). The higher applied force results in more contacts in the direction of the applied force.

It is important to note that most contacts are observed in the direction of the shear flow (**u**). At a shear rate of  $\tilde{\gamma} = 10^{-4}$  at  $\tilde{F} = 0.01$ , the axes of compression and extension are located at  $\theta = \pi/4$  and  $\theta = 5\pi/4$ , respectively. The contacts of the rigid particle are more apparent as observed in 8(A). Although there are more contacts, it does not necessarily mean the contacts are deeper. In fact,  $g(\tilde{r}, \theta)$  shows that the radial distance between two particles at contact is at

PLEASE CITE THIS ARTICLE AS DOI: 10.1063/5.0226758

Stability of rigid particle in yield stress fluids

the maximum at  $\theta = 5\pi/4$  (See Fig. 8(B)). Increasing the applied force to  $\tilde{F} = 1.00$  results in  $g(\tilde{x}, \tilde{y})$  showing contacts in the first and last quadrant. In this scenario, the particle is sedimenting in the direction of the flow, and that is observed in the velocity streamlines for this suspension (See 6(E)). Fig. 9 shows  $g(\tilde{x}, \tilde{y})$  and  $g(\tilde{r}, \theta)$  for the same suspensions undergoing a shear rate of  $\tilde{\gamma} = 10^{-7}$  at the same applied forces. Notably, Fig. 9(A) shows the formation of a more distinct ring-like structure around the center, which indicates areas of high particle contacts distributed uniformly between  $\pi < \theta < 2\pi$ . The depth of these contacts increases at large  $\tilde{F}$ , as seen in Fig. 9(C) where more contacts are observed in the direction of the applied force, indicating that there are more downward collisions than upward ones. In Fig. 9(B),  $g(\tilde{r}, \theta)$  shows that the contacts are more evenly distributed, while Fig. 9(D) shows that the contacts are in the sedimentation direction and in the last two quadrants ( $\pi \le \theta \le 2\pi$ ) and the radial distance between two particles at contact increases to a maximum of  $\theta = 5\pi/4$ . This, in return, shows how varying the shear rate and applied force significantly impact the microstructure of the particles in the vicinity of the sedimenting rigid particle.

## This is the author's peer reviewed, accepted manuscript. However, the online version of record will be different from this version once it has been copyedited and typeset. PLEASE CITE THIS ARTICLE AS DOI: 10.1063/5.0226758

Stability of rigid particle in yield stress fluids

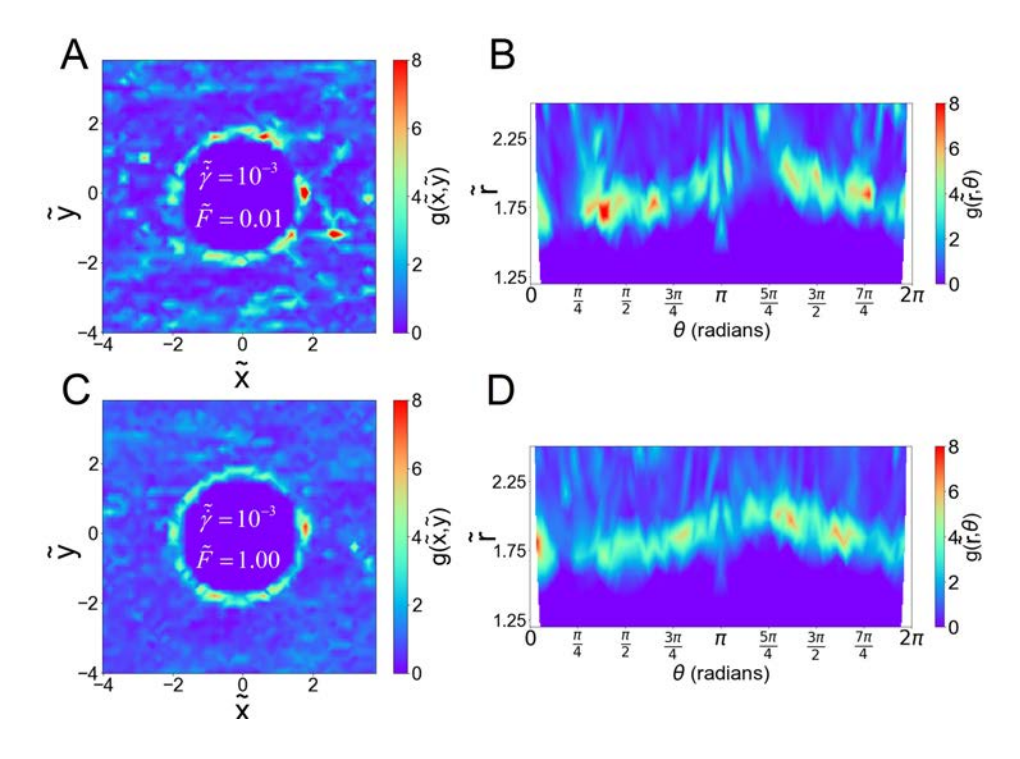


FIG. 7. 2-D pair distribution function,  $g(\tilde{x}, \tilde{y})$ , (A and C) and polar distribution function,  $g(\tilde{r}, \theta)$ , (B and D) at the vicinity of the rigid particle at a volume fraction  $\phi = 0.80$  undergoing (A)  $\tilde{\gamma} = 10^{-3}$  and  $\tilde{F} = 0.01$ , and (B)  $\tilde{\gamma} = 10^{-3}$  and  $\tilde{F} = 1.00$ .

PLEASE CITE THIS ARTICLE AS DOI: 10.1063/5.0226758

Stability of rigid particle in yield stress fluids

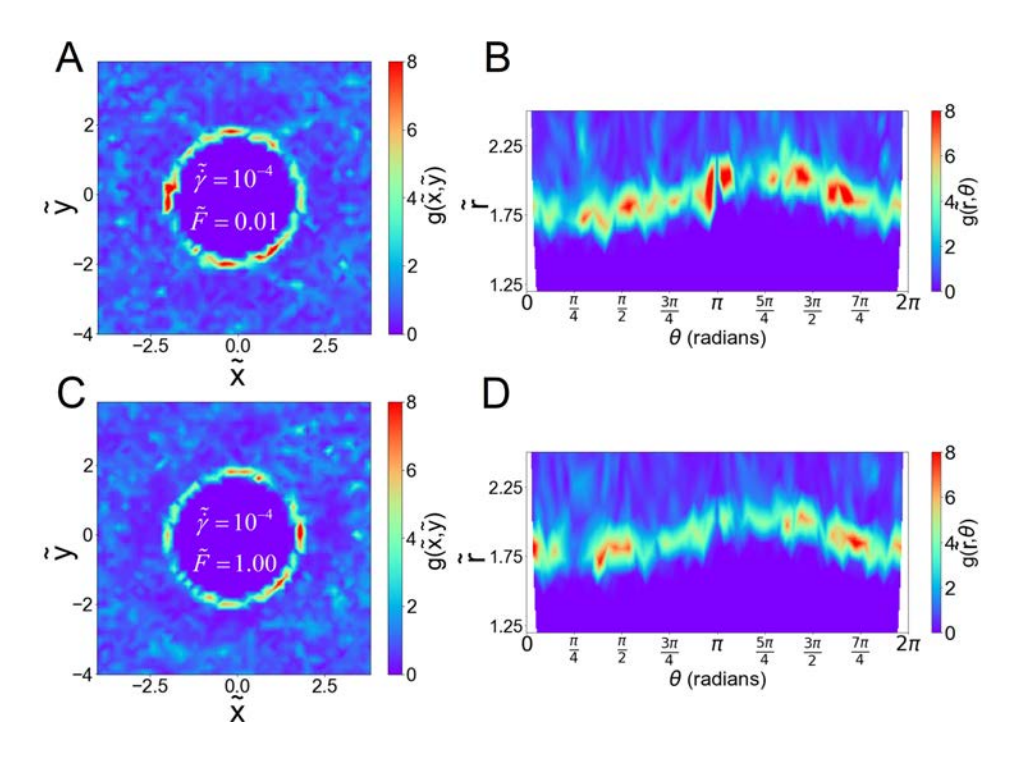


FIG. 8. 2-D pair distribution function,  $g(\tilde{x}, \tilde{y})$ , (A and C) and polar distribution function,  $g(\tilde{r}, \theta)$ , (B and D) at the vicinity of the rigid particle at a volume fraction  $\phi = 0.80$  undergoing (A)  $\tilde{\gamma} = 10^{-4}$  and  $\tilde{F} = 0.01$ , and (B)  $\tilde{\gamma} = 10^{-4}$  and  $\tilde{F} = 1.00$ .

PLEASE CITE THIS ARTICLE AS DOI: 10.1063/5.0226758

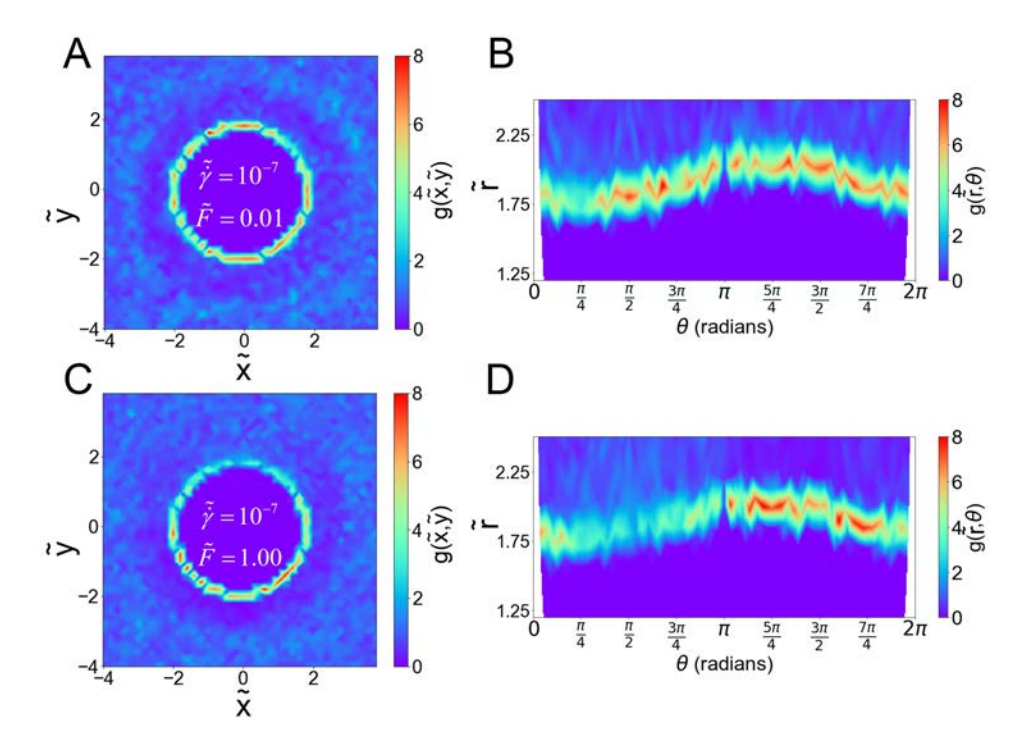


FIG. 9. 2-D pair distribution function,  $g(\tilde{x}, \tilde{y})$ ,(A and C) and polar distribution function,  $g(\tilde{r}, \theta)$ , (B and D) at the vicinity of the rigid particle at a volume fraction of  $\phi = 0.80$  undergoing (A)  $\tilde{\gamma} = 10^{-7}$  and  $\tilde{F} = 0.01$ , and (B)  $\tilde{\gamma} = 10^{-7}$  and  $\tilde{F} = 1.00$ .

To understand the dynamic behavior and rigid particle contacts, It is important to investigate the effect of shear flow on the residence time of the rigid particle in a local neighborhood of other SPGs. We determine the contact correlation function,  $C(\Delta \gamma)$ , over a strain interval of  $\Delta \gamma = \gamma - \gamma_0$ , in Fig.10, as

$$C(\Delta \gamma) = \frac{\langle H(\gamma_0 + \gamma)H(\gamma_0) \rangle}{\langle H(\gamma_0)^2 \rangle},\tag{8}$$

where H ( $\gamma$ ) = 1 if two rigid and soft particles are in contact; otherwise H ( $\gamma$ ) = 0. The decay of this function approximately corresponds to the duration over which particles within a suspension retain the memory of their contacts. At a shear rate of  $\tilde{\gamma} = 10^{-3}$  (Fig. 10(A)), it is observed that at a low force of  $\tilde{F} = 0.01$  (blue filled squares), the contacts are eventually remembered and the effective contact time plateaus.  $C(\Delta \gamma)$  decreases over very large strains and decays to zero

PLEASE CITE THIS ARTICLE AS DOI: 10.1063/5.0226758

slowly. Similarly, at a high force of  $\tilde{F}=1.00$  (green open circles), a similar behavior is observed, which confirms that the rigid particle has a localized motion at a high shear rate of  $\tilde{\gamma}=10^{-3}$  at both low and high applied forces. At a lower shear rate of  $\tilde{\gamma}=10^{-4}$  with the increase of force, the function goes to zero at an approximate strain of  $\gamma=10$  and the probability of two particles remaining in contact decays to zero, indicating a sedimenting particle (Fig. 10(B)). At a low force of  $\tilde{F}=0.01$  at  $\tilde{\gamma}=10^{-4}$  the decay over a long strain period is observed again, indicating that the suspension is stable. Finally, at a low shear rate of  $\tilde{\gamma}=10^{-7}$  where the rigid particle settles at the two applied forces, the decay at an applied force of  $\tilde{F}=0.01$ (blue open squares) and  $\tilde{F}=1.00$ (green open circles) happens rapidly, indicating that the suspension is unstable and the contacts are being forgotten quickly.

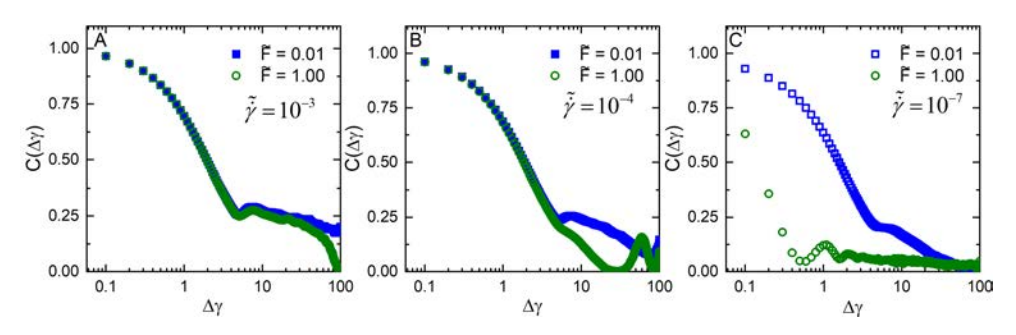


FIG. 10. Contact correlation function,  $C(\Delta\gamma)$ , between the rigid and soft particles in suspensions with volume fraction  $\phi=0.80$  and applied forces of  $\tilde{F}=0.01$  and  $\tilde{F}=1.00$  at shear rates of (A)  $\tilde{\gamma}=10^{-3}$ , (B)  $\tilde{\gamma}=10^{-4}$ , and (C)  $\tilde{\gamma}=10^{-7}$ .

## B. Stability diagram

There are three parameters that control the stability of the rigid particle in SPGs, *i.e.*, shear rate,  $\tilde{\gamma}$ , force acting on the particle,  $\tilde{F}$ , and volume fraction of the suspension,  $\phi$ . Thus, we construct stability diagrams of these suspensions by holding the volume fraction constant and varying  $\tilde{\gamma}$  and  $\tilde{F}$  (Fig. 11). When  $\phi=0.70$ , the stability diagram is dominated by sedimenting suspensions. The rigid particle shows stable behavior, *i.e.*, remains suspended in the SPGs only at high shear rates. At an increased volume fraction of  $\phi=0.80$ , more stable suspensions are obtained, indicating the evolution of stability of the increase in volume fraction (Fig. 11(B)). Finally, at  $\phi=0.90$ , the diagram is dominated by stable suspensions, indicating that an increase in the volume fraction leads to enhanced hindrance, which supports the stability of the suspension (Fig. 11(C)). The data

This is the author's peer reviewed, accepted manuscript. However, the online version of record will be different from this version once it has been copyedited and typeset. PLEASE CITE THIS ARTICLE AS DOI: 10.1063/5.0226758

suggest that as the SPGs are sheared, the shear forces exerted on the rigid particle increase and enhance stability. Therefore, it is crucial to determine a universal stability criterion at which one can control the sedimentation behavior in shear flow.

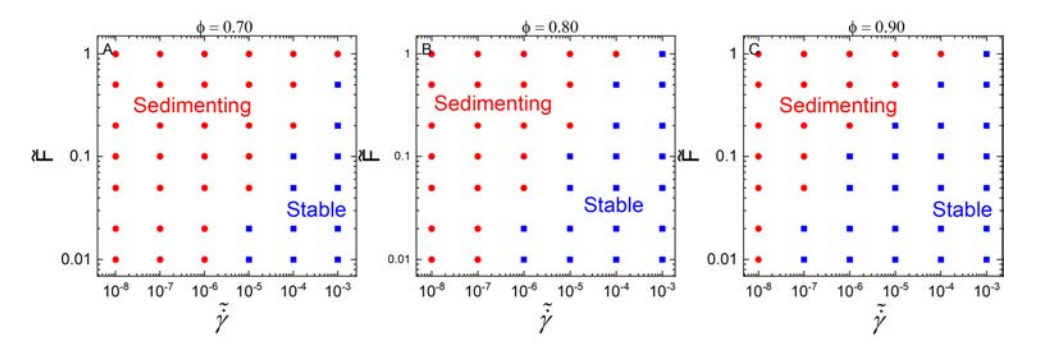


FIG. 11. Stability diagrams: Applied force,  $\tilde{F}$ , on the rigid particle as a function of shear rate,  $\tilde{\gamma}$ , at (A)  $\phi = 0.70$ , (B)  $\phi = 0.80$ , and (C)  $\phi = 0.90$ .

In the remainder of this paper, we propose a stability criterion for the shear-driven sedimentation of a rigid particle in SPGs. We also note the previous works reported experimentally<sup>23,42</sup> and theoretically<sup>43</sup> that a sphere at a quiescent condition in a yield stress fluid will not settle as long as  $\frac{\sigma_y}{\Delta \rho_g d} \ge \frac{1}{21}$ . Specific to SPGs, Mohan *et al.*<sup>25</sup> analyzed the forced motion of a tagged soft particle through a jammed suspension of SPGs where they report a stability threshold of  $O(G_0R^2)$ in a quiescent condition, where  $G_0$  is the low-frequency modulus of the paste and corresponds to cage elasticity.<sup>3</sup> Now, using the stability diagrams obtained at different volume fractions, a universal diagram is generated by scaling the shear rate with  $G_0/\eta_s$  (  $G_0$  is obtained by measuring the elastic moduli of the pastes when small amplitude oscillatory shear deformation is applied.<sup>3,7,44</sup>). Therefore, the dimensionless shear rate becomes  $\hat{\gamma} = \frac{\dot{\gamma}\eta_s}{G_0}$ ; note that  $\frac{\eta_s}{G_0}$  arises from the balance between viscous and elastic forces. 45 Furthermore, the external force is scaled by  $\sigma_y R^2$ , where  $\sigma_y$ values are obtained by fitting the flow curves to the Herschel-Bulkley model. 44 Thus, the dimensionless force becomes  $\hat{F} = \frac{F}{\sigma_v R^2}$ . Fig. 12 presents a stability diagram as a function of rescaled shear rate  $\hat{\gamma}$  and rescaled force,  $\hat{F}$  across different volume fractions. The plot distinctly marks the stability thresholds for each volume fraction with various symbols, where the spread in the data points illustrates the critical boundary between stable and unstable regimes. The solid black line in the figure represents a critical stability criterion, defined by the equation  $\hat{F} = C\hat{\gamma}^{0.57\pm0.07} + \hat{F}_{\nu}$ ,

PLEASE CITE THIS ARTICLE AS DOI: 10.1063/5.0226758

Stability of rigid particle in yield stress fluids

where C is 2174.33, and  $\hat{F}_{y}$  is a constant of 0.45. If the applied force is larger than this threshold, then the particle will sediment. This criterion also captures the quiescent condition (i.e.,  $\dot{\gamma} \rightarrow 0$ ) similar to that obtained by Mohan et al., where a critical force for particle motion in yield stress fluids must be exceeded for particles to overcome the local structure of their environment.<sup>25</sup> It is worth noting that the exponent determined here is close to the Herschel-Bulkley exponent of 0.51 obtained from the flow curve. 13 The similarity between these exponents suggests that the same underlying physical mechanisms—specifically the transition from a solid-like to a flow state under increasing stress—are at play in both the general flow behavior described by the Herschel-Bulkley equation and the specific stability dynamics observed in our study. This boundary line defines the necessary condition under which SPGs can maintain stability against sedimentation induced by external stresses.

This is the author's peer reviewed, accepted manuscript. However, the online version of record will be different from this version once it has been copyedited and typeset PLEASE CITE THIS ARTICLE AS DOI: 10.1063/5.0226758

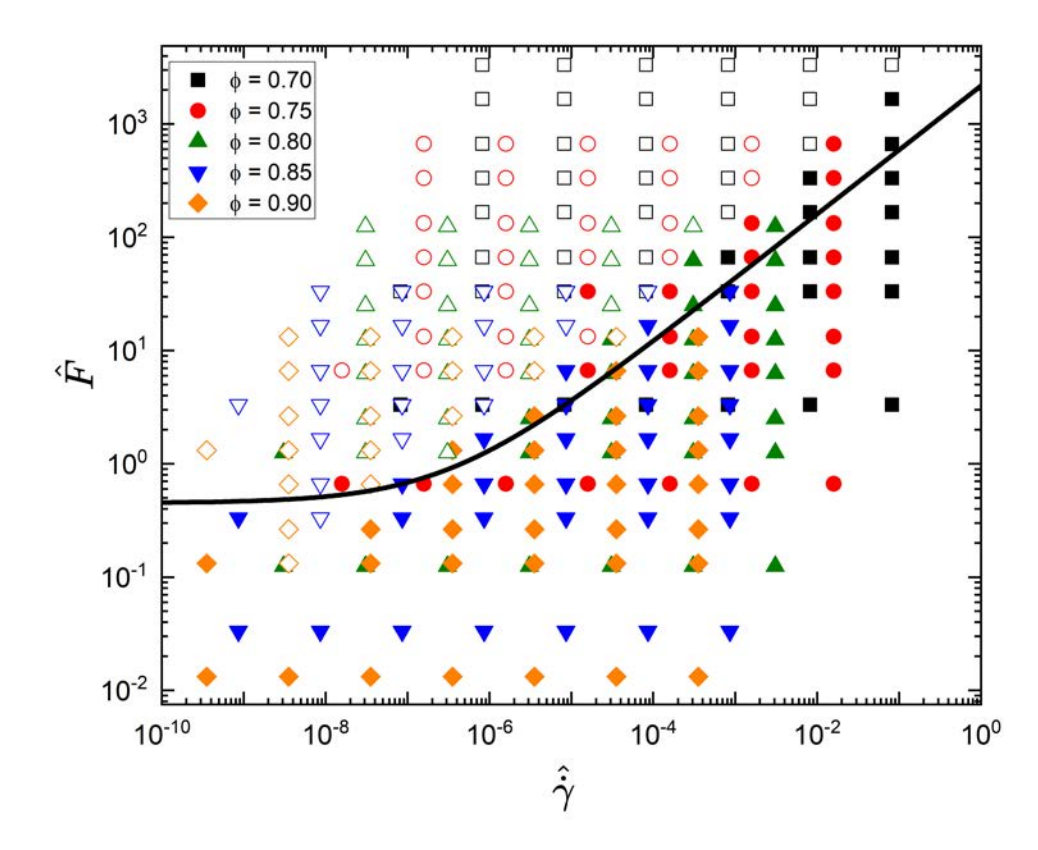


FIG. 12. Universal stability diagram: Rescaled applied force,  $\hat{F} = \frac{F}{\sigma_y R^2}$ , as a function of rescaled shear rate,  $\hat{\gamma} = \frac{\hat{\gamma} \eta_s}{G_0}$ . Open symbols: sedimenting, solid symbols: stable. The black line shows the stability criterion with an equation of  $\hat{F} = C\hat{\gamma}^{0.57\pm0.07} + \hat{F}_y$ .

## IV. Conclusions

In this study, the stability of a single rigid particle in SPGs, subjected to shear flow at different volume fractions, is explored. Critical parameters, such as shear rate, applied force on the rigid particle, and volume fraction of suspensions, govern the sedimentation behavior and stability of particles in dense suspensions. The analysis reveals that at a high shear rate and a low applied force on the rigid particle, the velocity field follows the a simple shear flow pattern. Conversely, at a low shear rate and a high applied force, the rigid particle sediments in the direction of the applied force and create a channel-like domain where sedimentation occurs.

PLEASE CITE THIS ARTICLE AS DOI: 10.1063/5.0226758

Stability of rigid particle in yield stress fluids

Similar to the experimental work done by Overlez *et al.*<sup>16,40</sup>, our results indicate that increasing the applied force increases the sedimentation velocity of the particle, which is evident at lower volume fractions where the SPGs are less resistant to particle movement. However, at high volume fractions, the dense packing of SPGs acts as a barrier, reducing the sedimentation rate. The mobility data highlight how the rigid particle affects the mobility across different shear rates and applied forces. This is also explained by considering that at the high rates, the suspension can sustain more load since the effective the shear stress of SPGs increases and a higher applied force on the rigid particle can be balanced by the fluid's stress. This, in return, restricts the particles' sedimentation. In contrast, at lower shear rates and higher applied forces, an increased particle displacement is observed, suggesting enhanced mobility and consequently, higher sedimentation chance.

The universal stability diagram shows how sedimentation is influenced by the interplay between shear rate, volume fraction, and applied force. This diagram illustrates the critical thresholds needed to maintain the stability of a rigid particle in SPGs. The establishment of a critical stability criterion, which expresses the minimum applied force rescaled with respect to the dynamic yield stress on the rigid particle as a function of flow strength, i.e.,  $\hat{F} = 2174.33 \hat{\gamma}^{0.57} + \hat{F}_y$ , underscores the ability to predict and manipulate the stability of suspensions under varying operational conditions. Similar to our work, The universal applicability of our scaling in comparison to others suggests that the underlying rheological behaviors governed by these parameters are intrinsically linked. In addition to practical applications, this work opens areas for studying the effects of particle shape, size distribution, and confinement on sedimentation behavior, similar to the works by Refs. 26 and 46.

## **Data Availability Statement**

Data are available upon reasonable request from the authors.

## **Conflicts of interest**

The authors have no conflicts to disclose.

## **Author Contributions**

Rakan Alrashdan: Conceptualization, investigation, visualization, formal analysis, Writing-first draft, Writing – review. Fardin Khabaz: Conceptualization, methodology, Writing – review & editing, funding acquisition, investigation, project administration.

PLEASE CITE THIS ARTICLE AS DOI: 10.1063/5.0226758

Stability of rigid particle in yield stress fluids

## Acknowledgment

RA and FK gratefully acknowledge support from NSF grants CBET-2240760 and NRT-2152210. The authors also acknowledge the Texas Advanced Computing Center (TACC) at the University of Texas at Austin for providing computational resources that contributed to the research results reported in this paper.

PLEASE CITE THIS ARTICLE AS DOI: 10.1063/5.0226758

Stability of rigid particle in yield stress fluids

## References

- <sup>1</sup>F. Khabaz, T. Liu, M. Cloitre, and R. T. Bonnecaze, "Shear-induced ordering and crystallization of jammed suspensions of soft particles glasses," Phys. Rev. Fluids. **2**, 093301 (2017).
- <sup>2</sup>F. Khabaz, M. Cloitre, and R. T. Bonnecaze, "Structural state diagram of concentrated suspensions of jammed soft particles in oscillatory shear flow," Phys. Rev. Fluids. **3**, 033301 (2018).
- <sup>3</sup>F. Khabaz, M. Cloitre, and R. T. Bonnecaze, "Particle dynamics predicts shear rheology of soft particle glasses," J. Rheol. **64**, 459–468 (2020).
- <sup>4</sup>F. Khabaz, B. F. Di Dio, M. Cloitre, and R. T. Bonnecaze, "Transient dynamics of soft particle glasses in startup shear flow. part i: Microstructure and time scales," J. Rheol. **65**, 241–255 (2021).
- <sup>5</sup>D. Vlassopoulos and M. Cloitre, "Tunable rheology of dense soft deformable colloids," Curr. Opin. Colloid Interface Sci. **19**, 561–574 (2014).
- <sup>6</sup>R. T. Bonnecaze and M. Cloitre, "Micromechanics of soft particle glasses," High Solid Dispersions, 117–161 (2010).
- <sup>7</sup>T. Liu, F. Khabaz, R. T. Bonnecaze, and M. Cloitre, "On the universality of the flow properties of soft-particle glasses," Soft Matter **14**, 7064–7074 (2018).
- <sup>8</sup>Y. Jiao, F. H. Stillinger, and S. Torquato, "Nonuniversality of density and disorder in jammed sphere packings," J. Appl. Phys. **109** (2011).
- <sup>9</sup>N. J. Wagner and J. F. Brady, "Shear thickening in colloidal dispersions," Phys. Today **62**, 27–32 (2009).
- <sup>10</sup>J. R. Seth, L. Mohan, C. Locatelli-Champagne, M. Cloitre, and R. T. Bonnecaze, "A micromechanical model to predict the flow of soft particle glasses," Nat. Mater. 10, 838–843 (2011).
- <sup>11</sup>R. Alrashdan, H. K. Yankah, M. Cloître, and F. Khabaz, "Shear-induced phase behavior of bidisperse jammed suspensions of soft particles," Physics of Fluids 36 (2024).
- <sup>12</sup>M. Cloitre, R. Borrega, F. Monti, and L. Leibler, "Glassy dynamics and flow properties of soft colloidal pastes," Phys. Rev. Lett. **90**, 068303 (2003).
- <sup>13</sup>H. Pable, N. Sadeghi, R. T. Bonnecaze, M. Cloitre, and F. Khabaz, "Microscopic signatures of heterogeneous flow in soft particle glasses," Submitted (2024).
- <sup>14</sup>L. Mohan, "Microstructure and rheology of soft particle glasses," (2013).
- <sup>15</sup>A. Fernandez-Nieves, H. Wyss, J. Mattsson, and D. A. Weitz, *Microgel suspensions: fundamentals and applications* (John Wiley & Sons, 2011).

PLEASE CITE THIS ARTICLE AS DOI: 10.1063/5.0226758

Stability of rigid particle in yield stress fluids

- <sup>16</sup>G. Ovarlez, F. Bertrand, P. Coussot, and X. Chateau, "Shear-induced sedimentation in yield stress fluids," J. Non-Newtonian Fluid Mech. 177, 19–28 (2012).
- <sup>17</sup>B. O. Torres Maldonado, R. Ran, K. L. Galloway, Q. Brosseau, S. Pradeep, and P. E. Arratia, "Phase separation during sedimentation of dilute bacterial suspensions," Phys. Fluids **34** (2022).
- <sup>18</sup>E. H. de Hoog, W. K. Kegel, A. van Blaaderen, and H. N. Lekkerkerker, "Direct observation of crystallization and aggregation in a phase-separating colloid-polymer suspension," Phys. Rev. E 64, 021407 (2001).
- <sup>19</sup>O. Torres, E. Andablo-Reyes, B. S. Murray, and A. Sarkar, "Emulsion microgel particles as high-performance bio-lubricants," ACS Appl. Mater. Interfaces 10, 26893–26905 (2018).
- <sup>20</sup>Z. Jaworski, T. Spychaj, A. Story, and G. Story, "Carbomer microgels as model yield-stress fluids," Rev. Chem. Eng. **38**, 881–919 (2022).
- <sup>21</sup>S. J. Stubley, *Design and rheological performance of microgel suspensions and microgel stabilised emulsions*, Ph.D. thesis, University of Leeds (2023).
- <sup>22</sup>J. F. Brady and L. J. Durlofsky, "The sedimentation rate of disordered suspensions," Phys. Fluids 31, 717–727 (1988).
- <sup>23</sup>H. Emady, M. Caggioni, and P. Spicer, "Colloidal microstructure effects on particle sedimentation in yield stress fluids," J. Rheol. **57**, 1761–1772 (2013).
- <sup>24</sup>M. Agarwal and Y. M. Joshi, "Signatures of physical aging and thixotropy in aqueous dispersion of carbopol," Phys. Fluids **31** (2019).
- <sup>25</sup>L. Mohan, M. Cloitre, and R. T. Bonnecaze, "Active microrheology of soft particle glasses," J. Rheol. 58, 1465–1482 (2014).
- <sup>26</sup>G. Ovarlez and E. Guazzelli, "Shear-induced migration of rigid spheres in a couette flow," (2024), hal-04510163.
- <sup>27</sup>M. Sarabian, M. E. Rosti, L. Brandt, and S. Hormozi, "Numerical simulations of a sphere settling in simple shear flows of yield stress fluids," J. Fluid Mech. 896, A17 (2020).
- <sup>28</sup>G. Ovarlez, F. Mahaut, S. Deboeuf, N. Lenoir, S. Hormozi, and X. Chateau, "Flows of suspensions of particles in yield stress fluids," J. Rheol. 59, 1449–1486 (2015).
- <sup>29</sup>A. Putz, T. Burghelea, I. Frigaard, and D. Martinez, "Settling of an isolated spherical particle in a yield stress shear thinning fluid," Phys. Fluids 20 (2008).
- <sup>30</sup>O. Merkak, L. Jossic, and A. Magnin, "Migration and sedimentation of spherical particles in a yield stress fluid flowing in a horizontal cylindrical pipe," AIChE journal 55, 2515–2525 (2009).

## PLEASE CITE THIS ARTICLE AS DOI: 10.1063/5.0226758

This is the author's peer reviewed, accepted manuscript. However, the online version of record will be different from this version once it has been copyedited and typeset.

Stability of rigid particle in yield stress fluids

- <sup>31</sup>R. Pal, "Modeling of sedimentation and creaming in suspensions and pickering emulsions," Fluids **4**, 186 (2019).
- <sup>32</sup>B. M. Berney and P. Deasy, "Evaluation of carbopol 934 as a suspending agent for sulphaoimidine suspensions," Int. J. Pharm. **3**, 73–80 (1979).
- <sup>33</sup>Y. Ali and K. Lehmussaari, "Industrial perspective in ocular drug delivery," Adv. Drug Delivery Rev. **58**, 1258–1268 (2006).
- <sup>34</sup>D. Praneta, N. Rutuja, S. Kamini, P. Bhagyashri, K. Divya, A. Kalyani, R. Satnam, and Y. Dipali, "Pharmaceutical suspensions: A review," Res. Rev.: J. Pharmacogn. Phytochem. 8, 952–955 (2019).
- <sup>35</sup>F. I. Abd-Allah, H. M. Dawaba, and A. M. Ahmed, "Preparation, characterization, and stability studies of piroxicam-loaded microemulsions in topical formulations," Drug Discov Ther 4, 267– 275 (2010).
- <sup>36</sup>M. M. Robins, "Emulsions—creaming phenomena," Curr. Opin. Colloid Interface Sci. 5, 265–272 (2000).
- <sup>37</sup>S. P. Meeker, R. T. Bonnecaze, and M. Cloitre, "Slip and flow in soft particle pastes," Phys. Rev. Lett. **92**, 198302 (2004).
- A. Lees and S. Edwards, "The computer study of transport processes under extreme conditions,"
   J. Phys. C: Solid State Phys. 5, 1921 (1972).
- <sup>39</sup>R. G. Larson, *The structure and rheology of complex fluids* (Oxford University Press, New York, USA, 1999).
- <sup>40</sup>G. Ovarlez, Q. Barral, and P. Coussot, "Three-dimensional jamming and flows of soft glassy materials," Nat. Mater. **9**, 115–119 (2010).
- <sup>41</sup>M. L. Falk and J. S. Langer, "Dynamics of viscoplastic deformation in amorphous solids," Phys. Rev. E 57, 7192 (1998).
- <sup>42</sup>A. Beris, J. Tsamopoulos, R. Armstrong, and R. Brown, "Creeping motion of a sphere through a bingham plastic," J. Fluid Mech. **158**, 219–244 (1985).
- <sup>43</sup>H. Tabuteau, P. Coussot, and J. R. de Bruyn, "Drag force on a sphere in steady motion through a yield-stress fluid," J. Rheol. **51**, 125–137 (2007).
- <sup>44</sup>N. Sadeghi, H. Pable, and F. Khabaz, "Thermodynamics description of startup flow of soft particles glasses," Soft Matter (2024).
- <sup>45</sup>B. F. Di Dio, F. Khabaz, R. T. Bonnecaze, and M. Cloitre, "Transient dynamics of soft particle glasses in startup shear flow. part ii: Memory and aging," J. Rheol. *66*, 717–730 (2022).

PLEASE CITE THIS ARTICLE AS DOI: 10.1063/5.0226758

Stability of rigid particle in yield stress fluids

<sup>46</sup>M. Sarabian, M. E. Rosti, and L. Brandt, "Interface-resolved simulations of the confinement effect on the sedimentation of a sphere in yield-stress fluids," J. Non-Newtonian Fluid Mech. 303, 104787 (2022).